Ocean Dynamics (2010) 60:883–900
DOI 10.1007/s10236-010-0302-6

Variability in Solomon Sea circulation derived from altimeter sea level data

Angélique Melet · Lionel Gourdeau · Jacques Verron

Received: 15 February 2010 / Accepted: 11 May 2010 / Published online: 5 June 2010

Abstract The Solomon Sea is a key region in the Pacific Ocean where equatorial and subtropical circulations are connected. The region exhibits the highest levels in sea level variability in the entire south tropical Pacific Ocean. Altimeter data was utilized to explore sea level and western boundary currents in this poorly understood portion of the ocean. Since the geography of the region is extremely intricate, with numerous islands and complex bathymetry, specifically reprocessed along-track data in addition to standard gridded data were utilized in this study. Sea level anomalies (SLA) in the Solomon Sea principally evolve at seasonal and interannual time scales. The annual cycle is phased by Rossby waves arriving in the Solomon Strait, whereas the interannual signature corresponds to the basin-scale ENSO mode. The highest SLA variability are concentrated in the eastern Solomon Sea, particularly at the mouth of the Solomon Strait, where they are associated with a high eddy kinetic energy signal that was particularly active during the phase transition during the 1997–1998 ENSO event. Track data appear especially helpful for documenting the fine structure of surface coastal currents. The annual variability of the boundary currents that emerged from altimetry compared quite well with the variability seen at the thermocline level, as based on numerical simulations. At interannual time scales, western boundary current transport anomalies counterbalance changes in western equatorial Pacific warm water volume, confirming the phasing of South Pacific western boundary currents to ENSO. Altimetry appears to be a valuable source of information for variability in low latitude western boundary currents and their associated transport in the South Pacific.

Keywords Southwest tropical Pacific Ocean · Solomon Sea · Altimetry · Low latitude western boundary currents · ENSO · Annual cycle

Responsible Editor: John Wilkin

A. Melet · J. Verron
LEGI, UMR 5519, CNRS & Grenoble Universités,
Grenoble, France

L. Gourdeau (✉)
UMR 5566, CNRS & IRD & Université Paul Sabatier,
Toulouse, France
e-mail: lionel.gourdeau@legos.obs-mip.fr

1 Introduction

The western sides of oceans are the site of intense boundary currents (WBCs) such as the Gulf Stream, the Kuroshio, and the East Australian Current, which close their respective subtropical gyres. They are highly energetic areas, easily revealed by altimetry (Wunsch and Stammer 1995). In a similar manner, the largest sea level variability in the entire tropical South Pacific Ocean is concentrated in the west where low latitude western boundary currents (LLWBCs) at the coast connect the subtropical region to the western equatorial Pacific (Fig. 1a).

Between 10°S and 5°S, the western South Pacific Ocean is comprised mainly of the Solomon Sea which is delineated by Papua New Guinea (PNG), New Britain (NB), and the Solomon Islands (SI; Fig. 1b). The sea is semi-enclosed and contains a complex bathymetry that is connected to the equatorial region through two main straits: the Vitiaz and the Solomon. The Solomon Sea is the final transit area for tropical waters flowing westward in the South Equatorial Current (SEC) and returning northward to the equator, in particular in the New Guinea Coastal Undercurrent (NGCU). The western boundary current, flowing along the PNG coast,

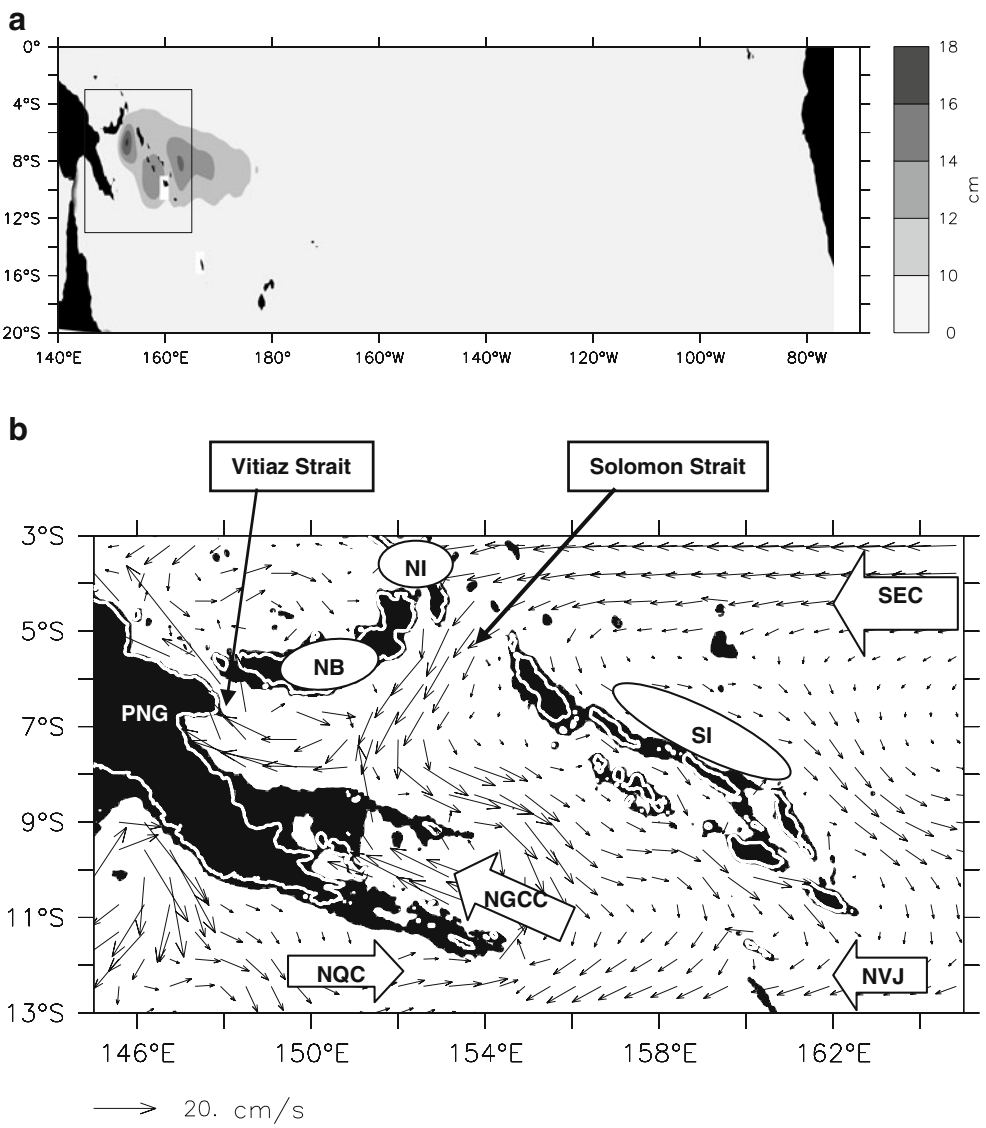

Fig. 1 **a** Sea level variability in the south tropical Pacific from AVISO gridded data for the November 1992 to December 2008 time period. The *rectangle* delimitates the region of interest. Units are shown in centimeters. **b** Mean surface circulation in the region of interest as provided by the 1/12° resolution primitive equation model. The land and the first 500 m oceanic depth are in *black*; the *white line* delineates the coastline. *PNG* Papua New Guinea, *NB* New Britain, *NI* New Ireland, *SI* Solomon Island, *SEC* South Equatorial Current, *NVJ* North Vanuatu Jet, *NQC* North Queensland Current, *NGCC* North Guinea Coastal Current

is a major source for the Equatorial Undercurrent (EUC) (Tsuchiya et al. 1989). Variability in advected water masses in this system can modulate the equatorial thermocline and ultimately the Pacific cold tongue and the atmospheric circulation, playing a major role in the low frequency modulation of ENSO (Schneider 2004; Yeager and Large 2004; Luo et al. 2005). Therefore, the Solomon Sea is of particular interest in a climatic context and is a focal point in the South Pacific Circulation and Climate Experiment (SPICE) program (http://www.clivar.org/organization/pacific/pacificSPICE.php).

Relatively few observations are available in this remote region of the world ocean. Some XBT measurements exist, from the Voluntary Observing Ships program, along commercial ship lines crossing the Solomon Sea, but sampling in these areas is too sparse to provide a useful description of this complex area. Some Argo floats have entered the Solomon Sea, but specific deployment of Argo floats are not actually planned in this region of very uneven bathymetry and strong currents. To document flow through the straits, Western Equatorial Pacific Ocean Climate Studies (WEPOCS) in 1985–1986 collected the first hydrographic and current meter measurements (Lindstrom et al. 1987, 1990). Vitiaz Strait data were also collected in 1992–1993 by mooring buoys in order to provide an estimate of transport variability over an annual cycle (Murray et al. 1995). An observational effort, supported by SPICE, is beginning. Recently, the FLUSEC1 cruise (Maes et al. 2009) provided the characterization of water masses entering the Solomon Sea during a single snapshot. Since 2007, gliders were regularly deployed in the Solomon Sea in order to monitor the entering current flux.

South of the Solomon Sea, the current system connecting the Coral Sea to the western equatorial Pacific is composed of the North Queensland Current (NQC) flowing northward along the Australia coast up to the Gulf of Papua

and the Solomon Sea and, to a lesser extent, by the North Vanuatu Jet (NVJ) that is formed by the splitting of the SEC at the northern tip of the Vanuatu archipelago (Qu and Lindstrom 2002; Kessler and Gourdeau 2007; Gourdeau et al. 2008). North of the Solomon Sea (along the PNG coast), the system is composed of the NGCU/NGCC currents. Both currents are described as flowing northwestward and evolve relatively in phase at annual and interannual time scales (Kuroda 2000; Ueki et al. 2003). If the core of the LLWBC is found in the subsurface in the NGCU, the NGCC (in the surface layers) exhibits higher variability. It is intensified during the boreal summer, then weakened or even reversed direction to southeastward during the boreal winter, in relation to seasonal variations of along shore monsoonal wind forcing (Tomczak and Godfrey 1993; Qu and Lindstrom 2002, Ueki et al. 2003).

In the Solomon Sea, the pathways of these currents are strongly constrained by bathymetric features and have been relatively unknown until now. In situ observational studies have shown that boundary currents have their core in the subsurface (Lindstrom et al. 1987, 1990; Butt and Lindstrom 1994; Murray et al. 1995). Using a high-resolution model analysis, Melet et al. (2010) proposed a scheme for thermocline circulation and detailed a double system of boundary currents. The main system flowing along the PNG coast was formed by the NGCU that permanently flows equatorward. One branch exited the Solomon Sea through the Vitiaz Strait, whereas the other, named the New Britain Coastal Undercurrent (NBCU), flowed eastward along the south coast of New Britain and exited through the Solomon Strait. The secondary LLWBC system flowed along the eastern side of the Solomon Islands and New Ireland. In the surface layers, the main NGCC branch enters the Solomon Sea through Milne Bay and escapes to the north through the few channels crossing the Woodlark before to exist at Vitiaz Strait (Fig. 1b). A SEC inflow enters the Solomon Sea via the Solomon Strait. A part of the SEC inflow directly circulates in the NGCC close to the Woodlark and another part re-circulates in the NVJ that is as strong as the NQC.

High sea level variability (Fig. 1a) and a high level of Eddy kinetic energy (EKE) (Qiu and Chen 2004) in the southwest tropical Pacific Ocean were a strong motivator for further exploring annual and interannual variability from sea level data in the Solomon Sea. Altimetry provides direct access to the sea level anomaly (SLA) signal. Sea level gradients also provide access to geostrophic current anomalies at the surface. Therefore, a part of the discussion here will focus on variability in the geostrophic component of the current system within the Solomon Sea, and especially on the signature of LLWBCs at the surface. Another part of the discussion will focus on the origin of various variability signals in time and space that emerge from altimetric analyses. A 1/12° resolution primitive equation model was utilized to provide an additional source of information to support and complement results derived from altimeter data.

The most readily available altimetric products provided by AVISO were gridded fields that merged satellite data from different altimetric missions including Topex/Poseidon (T/P) and ERS. Since complex bathymetry in the Solomon Sea was not taken into account during spatial interpolations and due to numerous amounts of flagged data in the coastal area, the product may be partly inappropriate for our study. For this reason, a complementary analysis using altimetric data was performed based on original along-track T/P data upon which specifically designed processing was performed.

The altimeter datasets that were used, obtained from the AVISO database and reprocessed along-track data, are first introduced in Section 2 along with the model description. The overall results for sea level variability in the Solomon Sea are presented in Section 3. Section 4 focuses on the variability related to LLWBCs. Section 5 focuses on high eddy activity within the Solomon Sea. The summary and conclusions are presented in Section 6.

2 Data and model

As mentioned previously, in order to study oceanic variability in this region which is relatively void of in situ data, altimetry products obtained through two complementary datasets were utilized: gridded AVISO data and along-track T/P data. The data was specifically reprocessed to provide reliable data near the coast or in shallow water. A 1/12° resolution primitive equation model, described below, provided additional information to support and complement physical interpretations derived from altimeter data.

2.1 Gridded AVISO data

Altimeter products distributed by AVISO, with the support of CNES (www.aviso.oceanobs.com), were the primary products utilized for this study. We considered a merged product that combined data from different altimetric missions. Depending upon time, up to four altimetry satellites were available (Jason1-2, Envisat or ERS1-2, Topex/Poseidon, and Geosat Follow On). ERS1-2 provided a finer spatial resolution than GFO and Topex/Poseidon/Jason1-2 (respectively, ~80, ~164, and ~315 km at the Equator and a coarser time resolution ~35, ~17, and ~10 days, respectively). A mapping procedure using optimal interpolation and realistic correlation functions was applied to produce SLA maps for a given date. Combining data from different missions significantly improved estimations of meso-scale signals (Pascual et al.

2006). SLA data were computed by referencing a 7-year average. The 1/3×1/3° gridded AVISO maps data were obtained every 7 days. The period under consideration ranged from November 1992 to December 2008. Despite limitations, as discussed in subsequent sections, gridded AVISO data were able to provide useful information in our study.

A look at the data showed that mapping did not take into account all of the numerous islands and that the data were often interpolated over the island chains that in reality formed significant barriers that separated different regimes. Additionally, it is known that standard altimetry products are not reliable near coasts and that the corresponding data are often skipped in datasets during quality control checks. The fact is that it is very difficult to adapt a standard procedure to apply valid geophysical corrections to the entire world's coastal ocean. Our motivation for developing another specific product (next section), dedicated to the Solomon Sea area, was to retrieve valid information near coasts.

2.2 Along-track DEGEO data

The second altimetric dataset employed in the study was built from original T/P GDR (Geophysical Data Record) data at a rate of 1/s, with a spacing of 6 km along the satellite track and collected between November 6, 1992 and August 6, 2002 (i.e., 360 passes; as distributed by AVISO). Only a few tracks crossing the Solomon Sea were selected (Fig. 2a). Original T/P data were reprocessed using the XTRACK processing chain (Roblou et al. 2007), developed by the Center for Topographic studies of the Oceans and Hydrosphere (CTOH/LEGOS, http://www.legos.obs-mip.fr/fr/observations/ctoh) dedicated to coastal applications. The reprocessing involves an ad hoc editing strategy of the data records and a careful extrapolation/interpolation of missing or defective corrective terms of the altimetric measurement in the coastal strip. Tidal corrections were derived from the higher-accuracy FES2004 model (Lyard et al. 2006). Oceanic high-frequency atmospheric-forcing response corrections were derived from the MOG2D model (Carrere

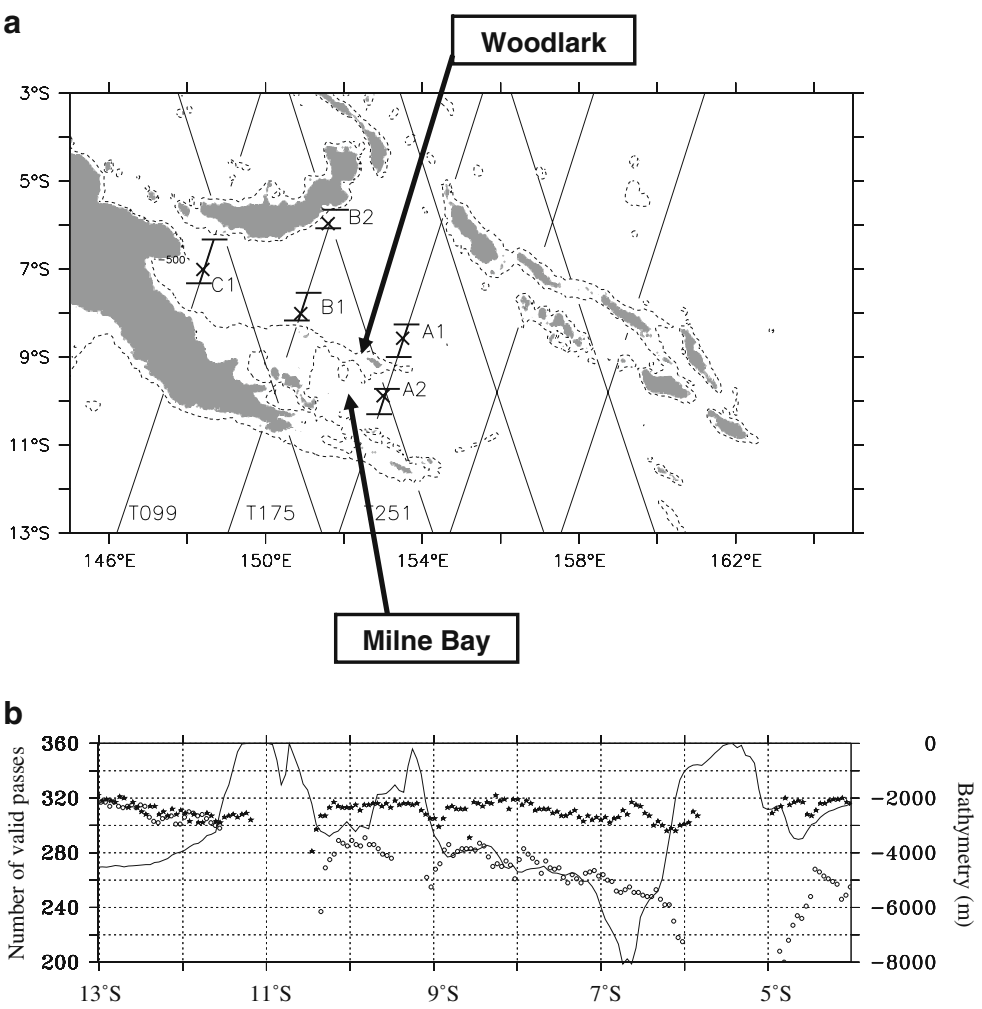

Fig. 2 **a** TOPEX/Poseidon tracks over the Solomon Sea. Three tracks (099, 175, and 251) were selected that were sufficiently orthogonal to the coast. The *dashed line* is the 500-m isobath. Cross-track LLWBCs are located by the *thick line*. *Crosses* are located at the point of maximum variability for the current. **b** A data processing example for track 251. The *black line* indicates bathymetry along the track. *White circles* and *black stars* show the number of valid cycles as a function of latitude for standard processing (AVISO product) and new processing (CTOH/LEGOS product), respectively

and Lyard 2003). Orbit errors were reduced by a stability criterion, and an inversion method was applied to derive a new high-resolution mean sea surface along the satellite's ground tracks. We also defined a more accurate and fine-scale land-sea mask to limit land contamination from the satellite footprint in coastal areas.

We post-processed the XTRACK altimetric SLA dataset to flag erroneous data using similar criteria as employed by Durand et al. (2008) for the East India Coastal Current. First, a four-sigma filter (sigma is referred to as the variance of SLA for a given altimetric point) and a two-sigma cycle-to-cycle difference filter was applied. Then, the data were relocated on a reference track corresponding to the barycenter of the 360 satellite groundtrack passes if available, thereby providing geographical corrections. A slope criterion was then applied in coastal regions. If the difference of the rms of the SLA between the altimetric point closer to the land than to its offshore neighbor was higher than 2 cm, the data of the coastal altimetric point was flagged and discarded. The filter was applied several times. An included data point must have had a minimum of 200 valid data passes within the 360 considered to be valid and not flagged. Finally, additional specific track-by-track subjective filtering was performed in order to remove erroneous data. Filtering consisted of an SLA variance threshold locally defined for each track and/or a bathymetric filter flagging all of the data points located in regions shallower than 500 m. The last filtering procedure was specific for each track, since no automatic procedure to remove erroneous data near coasts is currently available (to our knowledge).

The benefits of the new products in regards to AVISO data operational products are effective for individual tracks in terms of the numbers of valid data points (the number of cycles and the number of data points recovered along each individual track), especially near coastlines. The benefit of this new processing is illustrated, in an example, in Fig. 2b for track 251. In regard to the number of cycles, the gain was 6%, which equates to 21 more cycles than for AVISO data during the same time period.

2.3 Model

The 1/12° resolution model used in this study is described in detail in Melet et al. (2010). Therefore, only a brief description is provided here. In short, the high-resolution model is interactively nested (two-way nesting) in a 1/4° regional model of the southwest Pacific, which itself is embedded (open boundaries) into a global 1/4° global OGCM. The model formulation is based on standard primitive equations using a z vertical coordinate system. The model uses the NEMO numeric code, as utilized by several European Union laboratories (http://www.nemo-ocean.eu).

The primitive equations (PE) are discretized on an isotropic Arakawa C grid, using a Mercator projection. The vertical coordinate is geopotential with 46 prescribed z-levels ranging from the surface to 5,875 m (6 to 15 m vertical resolution in the upper 100 m). To improve the bathymetry representation with z-coordinates, a partial step parameterization is used to allow bottom cells depth to be adaptive and to differ from the vertical prescribed levels (Barnier et al. 2006). The model was forced by realistic winds and atmospheric temperature and humidity provided from the ECMWF ERA40 reanalysis (6 h fields). Precipitation (monthly fields) and long and short wave radiation (daily fields) were provided by the Common Ocean-ice Reference Experiments (CORE) dataset, developed by Yeager and Large (2004) at NCAR (Boulder, CO, USA).

3 Overall description

The following discussion reviews results obtained from gridded Aviso data products. The SLA averaged over the Solomon Sea showed a ±20 cm range in temporal variation during the 1992–2008 time period (Fig. 3a) with a clear annual signal that is strongly modulated on interannual timescales. A spectral analysis of the SLA time series exhibited three main peaks: one annual signal with a 5-cm magnitude (16% of the signal variance), and two interannual signals at a 2.5- and 5-year period with a 5- and 5.5-cm magnitude, respectively (not shown). Both annual and interannual timescales explained 63% of the signal variance.

Temporal variations in the SLA within the Solomon Sea looked very much like those observed both in the Bismark Sea (north of the Solomon Sea) and east of the Solomon Islands (not shown), suggesting that the Solomon Sea is part of the variability influencing the whole Southwest Pacific. Agreement within the open ocean south of 11°S was less obvious. The sharp phase shift in the annual cycle of wind stress curl at a latitude of 11°S (Kessler and Gourdeau 2007) that delimitates two different dynamic regimes should greatly contribute to the SLA difference between the Solomon Sea and the area away from its southern boundary.

Within the Solomon Sea, SLA spatial variability ranged between 6 and 16 cm rms, representing a well-marked spatial distribution with a clear distinction between the western and eastern Solomon Sea (Fig. 4a). The western Solomon Sea is characterized by relatively low SLA amplitudes, particularly near the coast where the main LLWBC system NGCC/NGCU currents flow along the main New Guinea shore. In contrast, the eastern Solomon Sea is characterized by relatively high SLA amplitudes. The highest level of variability, up to 16 cm rms, was quite

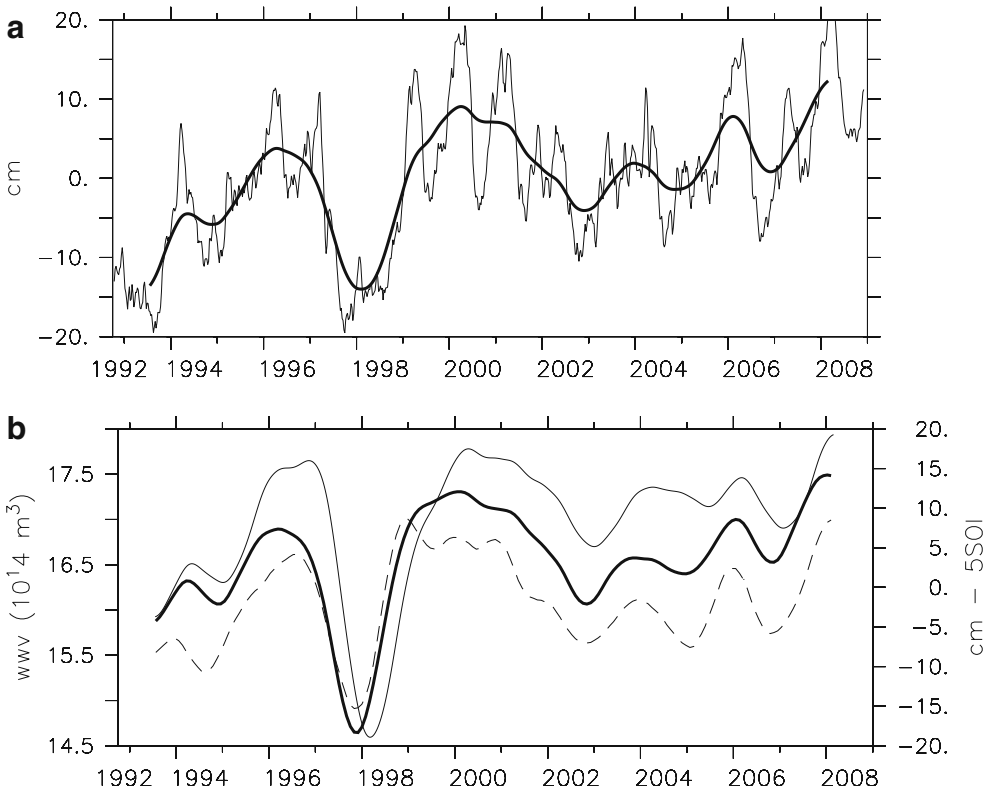

Fig. 3 **a** Time evolution of the SLA averaged for the Solomon Sea. Superimposed on the full signal (*thin line*) is the low pass filtered signal (*thick line*). The low pass filter has a half power at 18 months. Units are shown in centimeters. **b** The *dashed line* shows the South Oscillation Index (for convenience 5*SOI is plotted). The *thick line* shows the temporal function of EOF mode 1 computed from SLA over the tropical Pacific basin (15°S–15°N; in centimeter). The *thin line* shows the WWV changes in the Western tropical Pacific as defined by Meinen (2005) ($10^{14}m^3$). The different datasets have been low pass filtered according to the low pass filter SLA signal

localized in front of the Solomon Strait. High variability is in accordance with complex current recirculation that developed in the model for this area (Melet et al. 2010). The western and eastern Solomon Sea SLA signals are highly correlated (0.91 correlation) with their variability that varies from 5.6 to 10.4 cm rms, respectively. The difference in SLA variability between both basins is mostly explained by a dominant interannual signal in the eastern basin with a 8.1-cm rms against a 3.9-cm rms in the western basin.

EKE was computed from AVISO altimetric data through the classical formulation:

$$\mathrm{EKE} = 1/2(U'2 + V'2) \tag{1}$$

where U' and V' are the geostrophic current anomalies derived from SLA:

$$U' = -g/f\,\mathrm{dsla/dy} \tag{2}$$

$$V' = g/f\,\mathrm{dsla/dx} \tag{3}$$

where f is the Coriolis parameter, and g the gravity acceleration.

The EKE reached an average level of 419 cm^2/s^2 over the Solomon Sea, which is a high value compared to 242 cm^2/s^2 that was measured for a larger region by Qiu and Chen (2004). The EKE field showed that the smallest values are found in the western region, and that the highest values are principally located in the northeast part of the basin (as related to the previously mentioned patch of high SLA variability) and that it extends to the south in the mid-basin (Fig. 4b) following the SEC pathway (Fig. 1b). The EKE signal integrates the effects of both a meso-scale activity and also the low frequency variability of the current system, namely, the SEC inflow in that case (see Section 5).

Therefore, the Solomon Sea can roughly be divided into two main areas. The eastern and central basin is a turbulent area, especially in its north part where an SEC inflow enters the Solomon Sea at the Solomon strait (Fig. 1b). The highest EKE energy levels (1,000 cm^2/s^2) are found there and are equivalent to an rms velocity anomaly of 30 cm/s, whereas the western basin is dominated by a mean flow characteristic of LLWBC activity, with a core amplitude up to 60 cm/s at a depth of 200 m (Melet et al. 2010) and an annual sea level variability as strong as the interannual one.

3.1 Annual time scale

At annual time scales, the signature of the SLA in the Solomon Sea is at a maximum in March/April, at a minimum in August/September (Fig. 5a), and differs from the variability east of the Solomon Islands, where a remotely forced resonant Rossby wave regime dominates (Chen and Qiu 2004). The Rossby waves, generated in the east central Pacific, propagate to the west at the same speed as wind forcing. In the Solomon Sea, the phase of wind

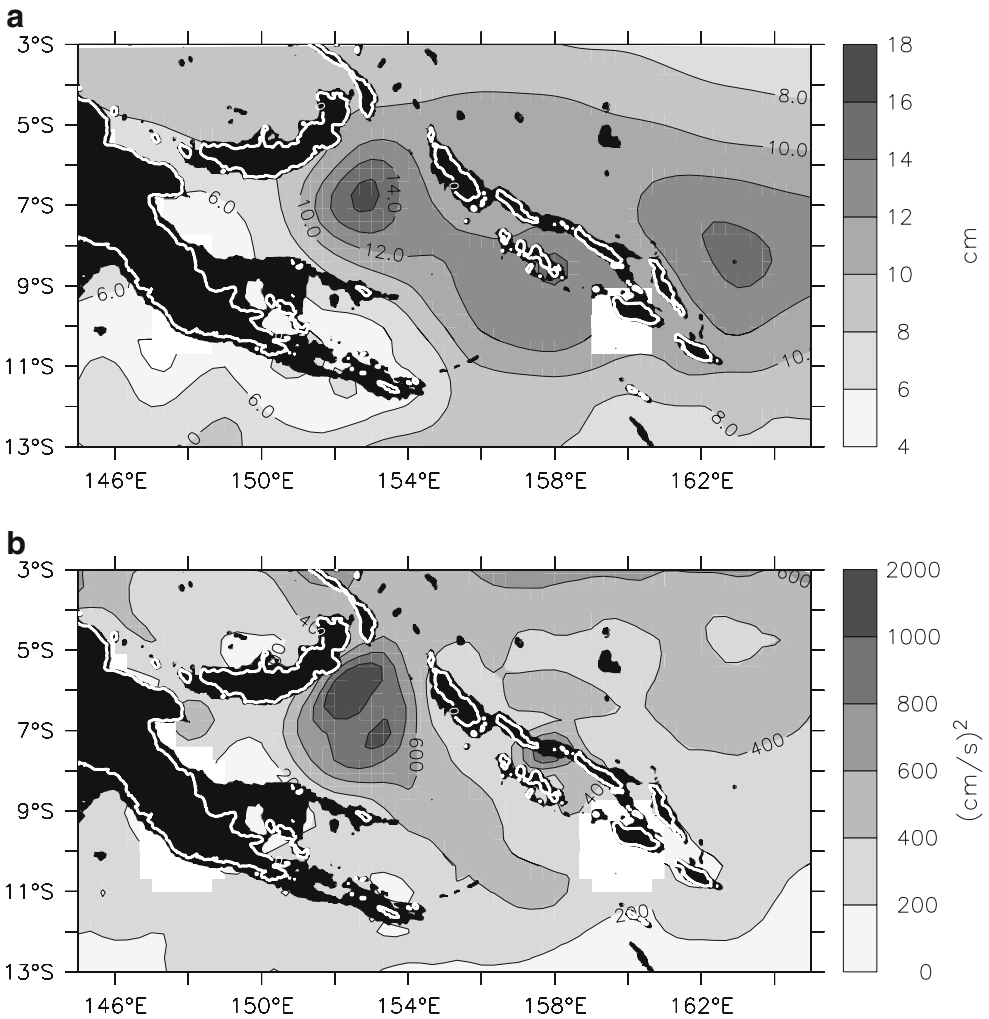

Fig. 4 **a** Map of the rms SLA variability over the Solomon Sea for the 1992–2008 period from the AVISO database. Units are shown in centimeters. **b** Eddy kinetic energy computed from the AVISO SLA database. Units are shown in cm^2/s^2. The land and the first 500 m oceanic depth are in *black*; the *white line* delineates the coastline

forcing matches that of the altimetric SLA with a 2-month lead (Fig. 5a), in good agreement with data from Chen and Qiu (2004) for the western basin. The Rossby waves impinge the Solomon Islands with a phase lag reflecting a decrease in the Rossby wave speed with latitude. Downwelling Rossby waves arrive at 6°S (the latitude of the Solomon Strait) in March to April (Fig. 5a), whereas the waves arrive at 11°S (latitude of Makira Island) in July to August (Fig. 5b). The Rossby wave signal at 11°S is lower than at 6°S, out of phase with the SLA signal in the Solomon Sea. The phase relationship between SLA variability in the Solomon Sea and Rossby waves at 6°S, with a 5–6-cm amplitude, argues for a strong connection between the Solomon Sea and the open ocean at the Solomon Strait. An analysis of the response of SLA variability in the Solomon Sea to local Ekman pumping (not shown) demonstrates that the maximum annual magnitude is around 2 cm. So, even if SLA variability in the Solomon Sea is a mix of response to local Ekman pumping and westward propagation of Rossby waves, the dominant signal is the westward propagation of Rossby waves arriving at Solomon Strait.

The SLA cycle induces a maximum southeastward surface geostrophic velocity anomaly during March to April in the Solomon Sea (Fig. 6) and indicates a decrease in the NGCC. South of the Solomon Sea, the eastward anomaly induces an increase in the NQC and a decrease in the NVJ. The opposite situation exists in August to September. In fact, when the NVJ is strong, it feeds water to the boundary such that both the NGCC anomaly is strong toward the equator (i.e., a NGCC increase), and the NQC anomaly is strong away from the equator (i.e., a NQC decrease). It is notable that the surface description determined from altimeter data provides similar conclusions as an analysis of OGCMs for a depth-averaged circulation in the southwest Pacific by Kessler and Gourdeau (2007) and for thermocline circulation in the Solomon Sea as determined by Melet et al. (2010). More details regarding the variability of LLWBCs are given in the next section.

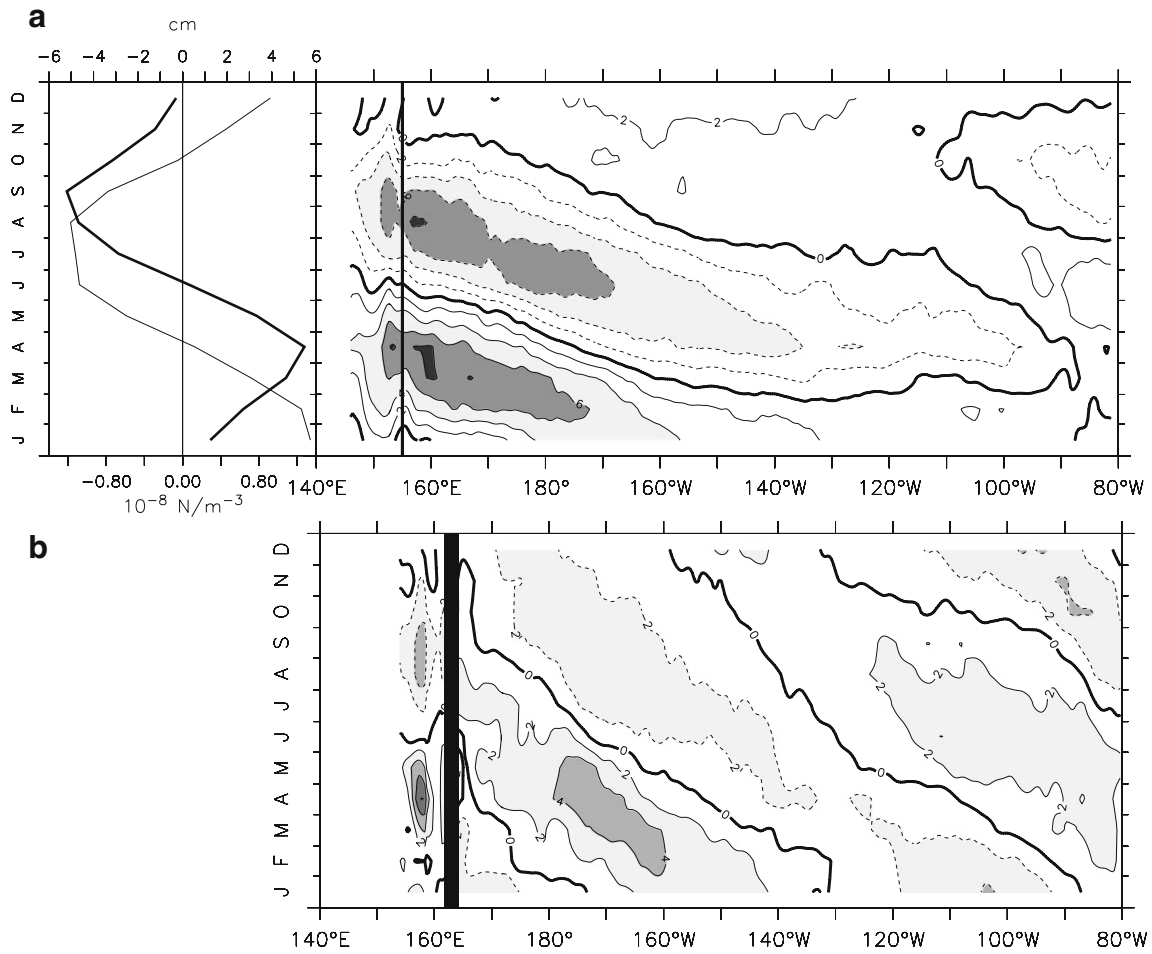

Fig. 5 **a** *Left*: the annual cycle of SLA (*thick line*), and the ERS wind stress curl (*thin line*) averaged over the Solomon Sea. *Right*: the time-longitude of the SLA in the 5–6°S latitudinal band over the Pacific. The location of the Solomon Strait is marked by the *thick line* at 155°E. **b** The time-longitude of the SLA in the 10–11°S latitudinal band over the Pacific. The location of the Solomon Islands is marked by the *thick line*. The contour intervals are 2 cm

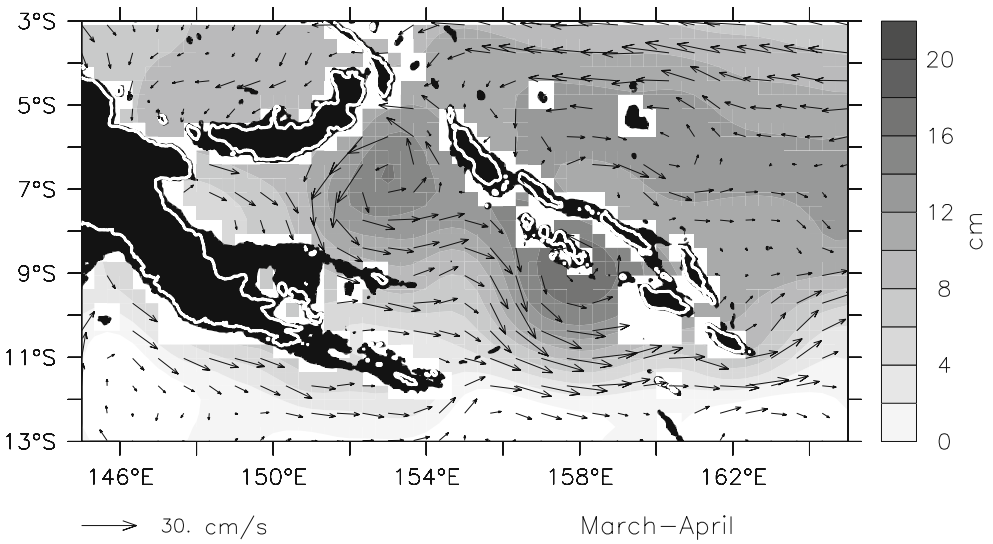

Fig. 6 Anomalies of the annual SLA signal for the March to April period from SLA AVISO gridded data are shown by *gray shading*. Superimposed are the corresponding surface geostrophic current anomalies for the March to April period. The land and the first 500 m oceanic depth are in *black*; the *white line* delineates the coastline

3.2 Interannual time scale

Let us recall what is observed at interannual time scale in the all-tropical Pacific. Two main EOF modes are representative of interannual sea level variability (Alory and Delcroix 2002). The first mode is the well-known ENSO mode characterized by a zonal tilt (Fig. 7a). The basin-scale first mode, in phase with ENSO, shows zonal migration of the warm pool and, as a consequence, expresses the warm water volume (≥20°C; Meinen and McPhaden 2001) changes in the western equatorial Pacific (WWVw (120°E–155°W; 5°S–5°N)). The second mode (not shown), characterized by a meridional seesaw centered at 5°N, is seen as a meridional recharge/discharge mode and leads ENSO by 7 months and expresses the warm water volume (WWV (120°E–95°W; 5°S–5°N)) exchanges between the equatorial Pacific Ocean and higher latitudes (Meinen and McPhaden 2001). Altimetric observations have already been utilized, with success, by Meinen (2005), to document WWV changes over the Pacific Ocean. It is the incompletely balanced meridional interior transport by western boundary currents which leads to low frequency changes in the WWV consistent with the oscillator as hypothesized by Jin (1997). Modeling studies have determined the net meridional transport (interior+LLWBC) in the equatorial Pacific (Lee and Fukumori 2003; Kug et al. 2003; Ishida et al. 2008), and most point out that these transports are highly influenced by meridional asymmetry between the northern and southern hemispheres. Antisymmetric characteristics are mainly due to a southward shift in the maximum zonal wind stress anomaly during the ENSO mature phase at the origin of strong wind stress curl in the South Western Pacific that generates large negative SLA. As a consequence, transports are stronger in the southern hemisphere than in the northern hemisphere, and in the southern hemisphere, most of the modeled interior transport is compensated by the LLWBC transport (Ishida et al. 2008; Lübbecke et al. 2008).

In the Solomon Sea, the interannual signal is the dominant signal and is directly related to ENSO activity, represented here by the SOI index (Fig. 3b). An EOF analysis of the Solomon Sea SLA indicated that 96% of the variance in the low frequency signal (half power at 18 months) was explained by one mode. Spatially, this regional mode looks like the basin-scale ENSO mode in the Solomon Sea; its time series greatly resembles that of the

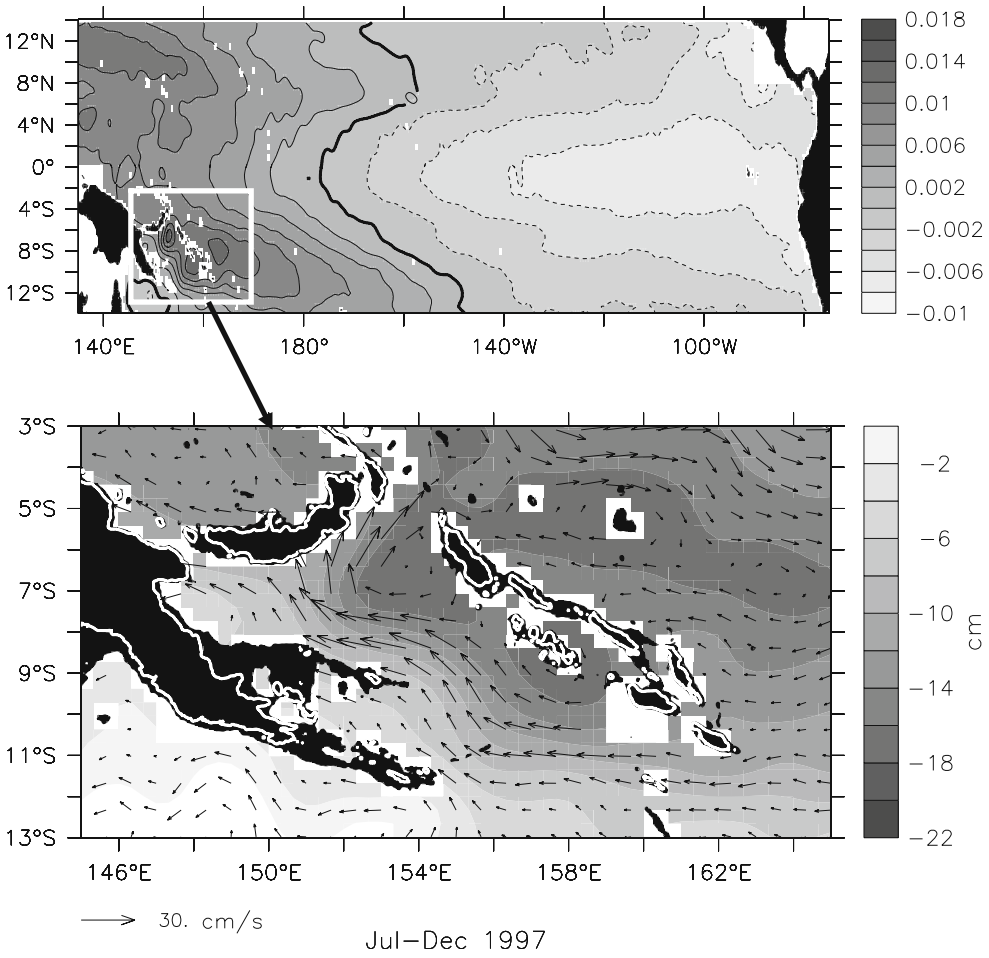

Fig. 7 **a** EOF mode 1 from SLA AVISO gridded data for the tropical Pacific. **b** The low pass filtered (half power at 18 months) SLA anomalies during the 1997 El Niño averaged for the July to December 1997 period are in *gray shading*. Superimposed is the corresponding anomalies of surface geostrophic currents. The land and the first 500 m oceanic depth are in *black*; the *white line* delineates the coastline

time series for the basin-scale ENSO mode described above (Fig. 3b), indicating that a strong relationship exists between WWVw changes in the western equatorial Pacific, sea level variability in the Solomon Sea, and corresponding changes in strength in South Pacific LLWBCs, as will be discussed in the next section. During the period under consideration, the major event was the 1997–1998 ENSO with a negative 15-cm SLA over the Solomon Sea.

As illustrated by the ENSO mode, a signature for the 1997 El Niño, during the period July to December 1997, was the large patch of negative SLA extending on each side of the Solomon Islands that induced SLA gradients at the origin of surface geostrophic velocity anomalies (Fig. 7b). Offshore of the Solomon Sea, southeastward velocity anomalies developed north of 7°S in coordination with the depletion of WWVw, whereas westward velocity anomalies developed south of 10°S increasing the NVJ. Most of the anomalies turned northwestward in the Solomon Sea, increasing the NGCC, whereas a small part extended to the Australian coast, decreasing the NQC and suggesting that at the surface, the Australian LLWBCs could mainly be controlled by the SEC inflow around 10°S, not only at the annual time scale as shown by Kessler and Gourdeau (2007) but also at an interannual time scale. In the Solomon Sea, northwestward surface geostrophic flow anomalies as high as 20 cm/s are mainly located in the western Solomon Sea. The anomalies bifurcate at the New Britain coast before escaping through the Vitiaz and Solomon Straits. Therefore, LLWBCs flowing in the Solomon Sea are reinforced during the growing phase of El Niño to fill the western equatorial Pacific when the WWVw decreases due to a divergence of the interior flow. The surface description from altimetry confirms the role of the Solomon Sea as the pathway of LLWBC anomalies in phase opposition with interior geostrophic flow as pointed out by several model studies (Kug et al. 2003; Ishida et al. 2008).

To summarize, at seasonal and interannual time scales, the SLA evolves in phase in the Solomon Sea. The highest SLA variability is concentrated in the eastern Solomon Sea, particularly at the mouth of the Solomon Strait where it is associated with a high EKE signal. The marked asymmetry in the SLA amplitude between the eastern and western Solomon Sea generates SLA gradients that produce surface geostrophic current anomalies in the Solomon Sea. The anomalous circulation within the Solomon Sea is principally related to one of the LLWBCs. The SLA annual cycle seems to be highly influenced by Rossby waves at the Solomon Strait. During austral autumn (spring), the SLA is at a maximum (minimum), and the surface geostrophic velocity anomalies show an exiting (entering) flow at the southern Solomon Sea boundary. On an interannual time scale, the Solomon Sea SLA signature corresponds to the basin-scale first ENSO mode. Surface geostrophic velocity anomalies from altimetry confirm the role of the Solomon Sea as the pathway of LLWBC anomalies in phase opposition with the interior geostrophic flow.

In the next two sections, we detail the variability in the LLWBC on the western side of the basin, and eddy activity on the eastern side of the basin.

4 Variability in the western Solomon Sea: the LLWBCs

LLWBCs in the Solomon Sea refer to the NGCC/NGCU current system that is highly constrained by topographic features. Such structures cannot be well depicted from the gridded AVISO dataset. Along-track data that we have processed in coastal areas (see Section 2) are used to document variations at the surface of the Solomon Sea LLWBCs at annual and interannual time scales, assuming that alongshore flow is in geostrophic balance. The first step was to localize these thin coastal currents. We selected three descending tracks “251, 175, and 99” that were sufficiently orthogonal to the coast to favorably determine alongshore currents (Fig. 2a). Track T/P251 crossed Milne Bay and the eastern tip of the Woodlark Islands. Further west, track T/P175 sampled the northern shelf break of the Woodlark Islands and reached the southern coast of New Britain. Track T/P099 sampled the area at the mouth of the Vitiaz Strait. Cross-track geostrophic current anomalies were derived from along-track SLA gradients. Data gaps were small enough to adequately resolve periods greater than 2 months. Our dataset allowed the monitoring of the variability of boundary currents to within a few kilometers of the shore, defined as the shelf break intersecting the 500-m isobath. Hovmuller plots of the along-track current anomalies show a coherent signal extending off the coast at annual time scale (not shown) that we consider as the signature of the LLWBCs. To accurately define the LLWBCs along the track, the maximal annual current variability is located from the coast, and the geographical extension of the LLWBCs is defined as the region in which correlations with the point of maximal annual variability are larger than 0.85 (an example for T/P251 is shown in Fig. 8). In the following, LLWBC anomalies are defined as current anomalies averaged over the pre-defined width of the LLWBC. Cross-track boundary currents are located in Fig. 2a, and their characteristics are detailed in Table 1. A clear annual signature of currents was detected in Milne Bay (A2), along the Woodlark (A1, B1), at the mouth of the Vitiaz Strait (C1), and at the New Britain coast (B2). The typical width of the currents was around 70 km, except at the Vitiaz Strait where it was wider (100 km) and at the New Britain coast where it was only 50 km wide.

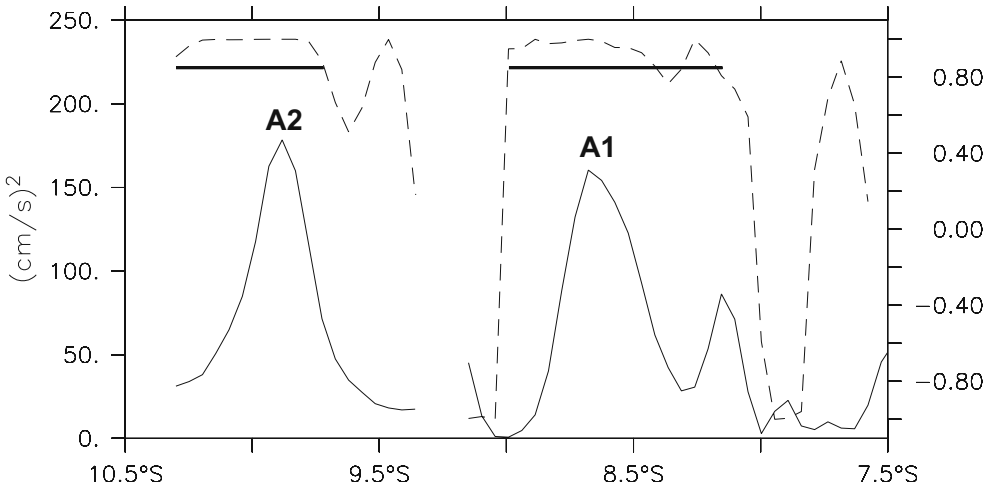

Fig. 8 The variance of annual current variability (continuous line, in cm^2/s^2) is plotted for the T/P251 track as a function of latitude. The hole at approximately 9.2°S indicates Woodlark Island. A1 and A2 locate the points of maximal annual variability near the coast that make reference to the currents found at the eastern tip of Woodlark and in the Milne Bay, respectively, as shown in Fig. 2a. The correlation with the point of the maximum variability is shown by a *dashed line*. The width of the current is defined as the region in which the correlation is larger than 0.85 (*thick line*)

4.1 Annual variability

The annual cycle of boundary currents exhibited different amplitudes and phases (Fig. 9a) that illustrate the complex circulation at the surface (Fig. 1b). The LLWBCs at A2, B1, and C1 are located in the northward flux composed of the NGCC/NGCU current system, whereas the LLWBC at A1 is located in the southward flux from the SEC overlaying the NGCU. At the New Britain coast, The LLWBC at B2 does not correspond to a well-defined mean surface current although it overlays the NBCU. The NGCC amplitude varied from 15 cm/s in Milne Bay (A2) to 25 cm/s at the Vitiaz Strait, and according to Table 1, their respective transport anomalies at the surface varied from 10^4 to $3.10^4 m^2/s$ according to the definition of the LLWBCs in Table 1. The NGCC flowing into Milne bay (A2) was at a minimum in March and at a maximum in September and was in phase with the NGCC north of Woodlark (B1). At the Vitiaz Strait, the NGCC (C1) leads the NGCC in Milne Bay (A2) by 1–2 months. The minimum occurred in February, and the maximum occurred in August and was phased with the variability at the eastern tip of the Woodlark (A1). Variability at the New Britain coast (B2) was in phase opposition with the NGCC at Woodlark (B1), meaning that when the NGCC increases (decrease), eastward (westward) current anomalies to the Solomon strait developed at the surface along the New Britain coast.

The different phase relationship between LLWBCs at the surface based on altimetry were consistent with the seasonal cycle of the LLWBCs at the thermocline level as analyzed in the study of (Melet et al. 2010). For instance, in Milne Bay, the NGCU was at a maximum in October, phased with the NBCU, whereas the eastern part of the NGCU flowing in the central basin was advanced and phased with the NGCU branch of the Vitiaz Strait (maximum in August). The strongest annual variability of the NGCC transport located at the mouth of the Vitiaz strait resembled the NGCC variability north of PNG described as a response to the local along shore monsoonal wind (Kuroda 2000; Ueki et al. 2003). The monsoonal wind affects only the surface layers and could not explain the good correlation between variability at the surface and in the subsurface described here. It indicates that if the signal at Vitiaz was consistent with different sources of variability, the variability of the LLWBCs, which have their core in the subsurface at the level of the thermocline (Melet et al. 2010), has a strong geostrophic signature at the surface detectable from altimetry.

Table 1 The location and characteristics of different coastal currents located along the altimeter tracks, as presented in Fig. 2a

	A1 153.5°E; 8.6°S	A2 153°E; 9.8°S	B1 150.9°E; 8°S	B2 151.6°E; 6°S	C1 148.4°E, 7°S
Width (km)	85	68	77	52	119
Amplitude annual cycle (cm/s)	10	15	18	15	25

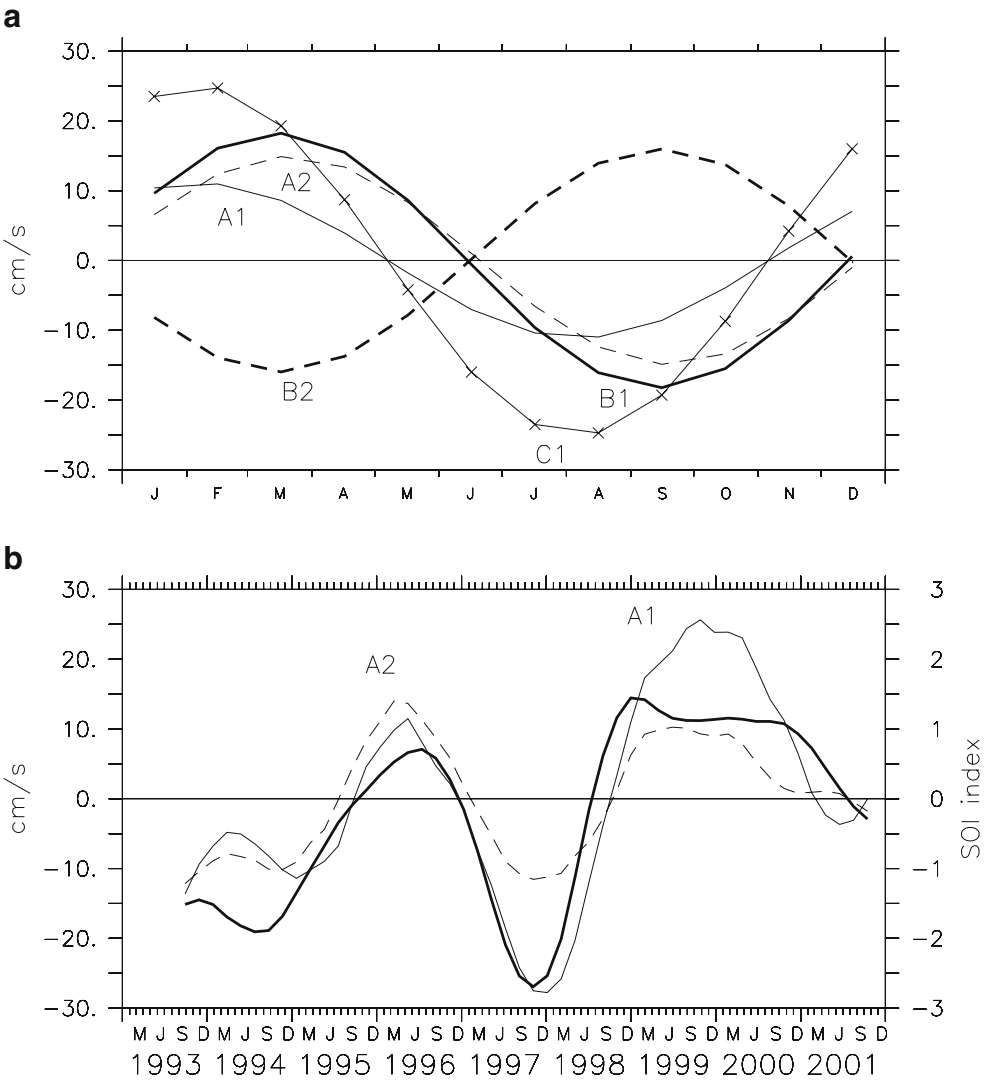

Fig. 9 **a** Annual variation for LLWBCs at the various locations defined in Fig. 2a (A1: *thin line*; A2: *thin dash line*; B1: *thick line*; B2: *thick dash line*; C1: *line with crosses*). Negative anomalies are westward anomalies (unit are centimeters per second). **b** Interannual variation for LLWBCs at A1 (*thin line*) and A2 (*dashed line*; unit are centimeters per second). Superimposed on the figure is the SOI index (*thick line*)

4.2 Interannual variability

As sea level responds to ENSO (Fig. 3b), altimetry can help to determine the interannual response of LLWBCs in the southwestern Pacific boundary. Ridgway et al. (1993) first studied the sea level response in the Solomon Sea due to the 1986–1987 ENSO, thanks to in situ tide gauges and XBT data. They provided estimation of anomalous geostrophic transport anomalies (Ta) in the Solomon Sea by using the simple expression:

$$\mathrm{Ta} = g\mathrm{d}HD/f \tag{4}$$

where dH is the sea level difference from tide gauges between Port Moresby (PNG) and Honiara (Solomon Island), and D is an e-folding depth of 150 m for the anomalous current approximated using XBT data.

Here, we apply the same formula using altimetry in regard to the current anomalies described above. The same D as that in Ridgway et al. (1993) was utilized. Along-track data or AVISO gridded data provided similar transport anomalies (not shown), and we preferentially used the longest time series from AVISO gridded data. The estimation of low frequency transport anomalies was validated against the model outputs from both the modelled velocity, integrated from the surface down to 150 m depth and SLA fields. Both estimations provided relatively similar results for transport anomalies at the south boundary of the Solomon Sea between the PNG and the Solomon Islands, as shown in Fig. 10. The results indicate that surface variability is a good proxy for estimating a depth integrated transport anomaly. Also, a comparison with the total transport integrated from the surface to the bottom indicates that most of the variability is in the surface layers. Therefore, as applied to altimetric data, this method could be useful for monitoring transport anomalies.

Between the PNG and the Solomon Islands, transport anomalies at the southern boundary of the Solomon Sea were closely related to ENSO (Fig. 11a). Positive anomalies

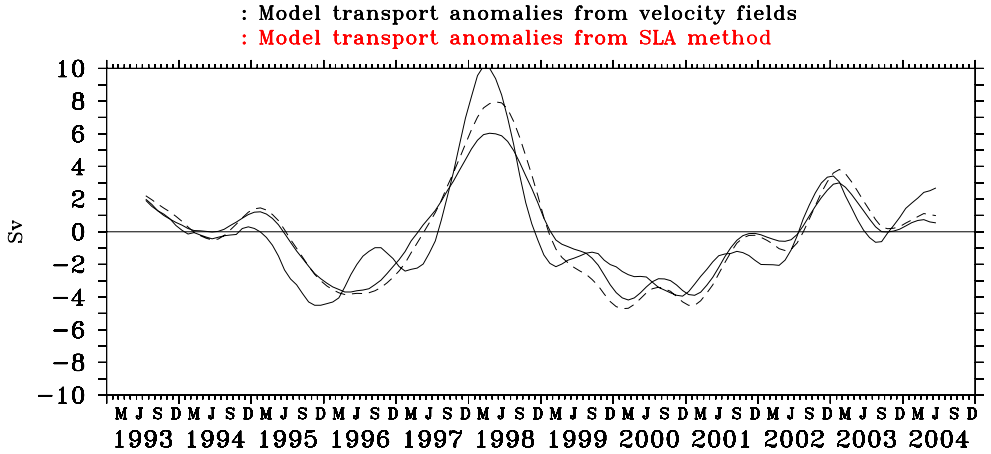

Fig. 10 Model results showing transport anomalies at the southern boundary of the Solomon Sea computed by (1) the SLA difference between PNG and Solomon Island using an e-folding depth of 150 m (*dashed line*), (2) the velocity field of the model integrated from the surface to a depth of 150 m (*thick line*), and (3) the velocity field of the model integrated from the surface to the bottom (*continuous line*). Units are shown in Sv

were observed in 1994, 1997, 2002, 2004, and 2006 in relation to El Niño events, and negative anomalies associated with La Niña events were observed in 1995–1996, 1998–2000, and 2007–2008. The transport anomalies reaches 8 Sv during the 1997–1998 ENSO event, and since 2002, the signal had a clear biannual period. Transport anomalies in the Solomon Sea are intimately linked to the temporal variation of the WWVw (dWWVw/dt) both in terms of phase and amplitude. Most of the time, both curves were anti-correlated except during the transition phase between the 1997 El Niño and the 1998 La Niña. In fact, dWWVw/dt lead the LLWBC variability by approximately 4 months with an anti-correlation as high as −0.7 indicating that WWVw changes drive variations in the transport within the Solomon Sea that, in return, counterbalance most of the WWVw changes.

The transport anomalies were principally associated with transport anomalies of the LLWBCs. As previously mentioned, LLWBCs entering the Solomon Sea were divided into a flow in Milne Bay (A2) and a flow arriving at the eastern tip of the Woodlark (A1). Both boundary currents evolve in the same way in phase with the SOI (Fig. 9b). Variations in the currents were higher at the eastern tip of Woodlark (A1) with a maximum amplitude up to 30 cm/s in December 1997. In Milne Bay, the maximum amplitude was only 10 cm/s. Transport anomalies relative to each current were estimated by projecting the surface information and summed to provide an estimation for transport variability. An e-folding depth of 200 m, corresponding to the depth in the core of the LLWBCs (Melet et al. 2010), was found to give the best comparison with estimations of transport between the PNG and the Solomon Islands. The transport variability of the LLWBCs was very close to the one estimated by the SLA difference at the south entrance of the Solomon Sea (Fig. 11a). Therefore, if the SLA difference is a relatively simple way to monitor interannual transport anomalies in the Solomon Sea, it is also possible to follow the partition of the signal between different pathways (Milne Bay versus the eastern tip of Woodlark).

Like at the south boundary of the Solomon Sea, the transport anomalies at the Vitiaz and Solomon straits are estimated (Fig. 11b). As expected, the sum of the transport anomalies at both straits balances the transport at the south boundary (Fig. 11a). The highest anomalies were observed at the Solomon strait and reached 6 Sv, whereas at the Vitiaz Strait, the anomalies were less than 4 Sv even during the 1997–1998 ENSO. Anomalies of transport at the Solomon strait were relatively well phased with dWWVw/dt and lead the transport anomalies at the Vitiaz strait by approximately 9 months except during the 1997–1998 ENSO event, suggesting atypical character for this major event. During the 1997 El Niño, both of the transports at the Solomon and the Vitiaz straits were in phase to balance the huge anomaly of transports entering the Solomon Sea on the south. During the 1998 La Niña, equatorward flow exiting the Solomon Sea continues to prevail (Fig. 11a) and participates with westward transport anomalies in the equatorial band (associated with La Niña condition) to a drastic increase in dWWVw/dt in the western equatorial Pacific that breaks the particular phase relationship between anomalous transport n the Solomon Sea and dWWWw/dt described above.

To summarize, LLWBCs are detected at the surface from an analysis of along-track SLA data. Both at annual and interannual time scales, their variability is highly related to the main LLWBCs flowing at depth. It means that if numerous vertical modes are necessary to describe the

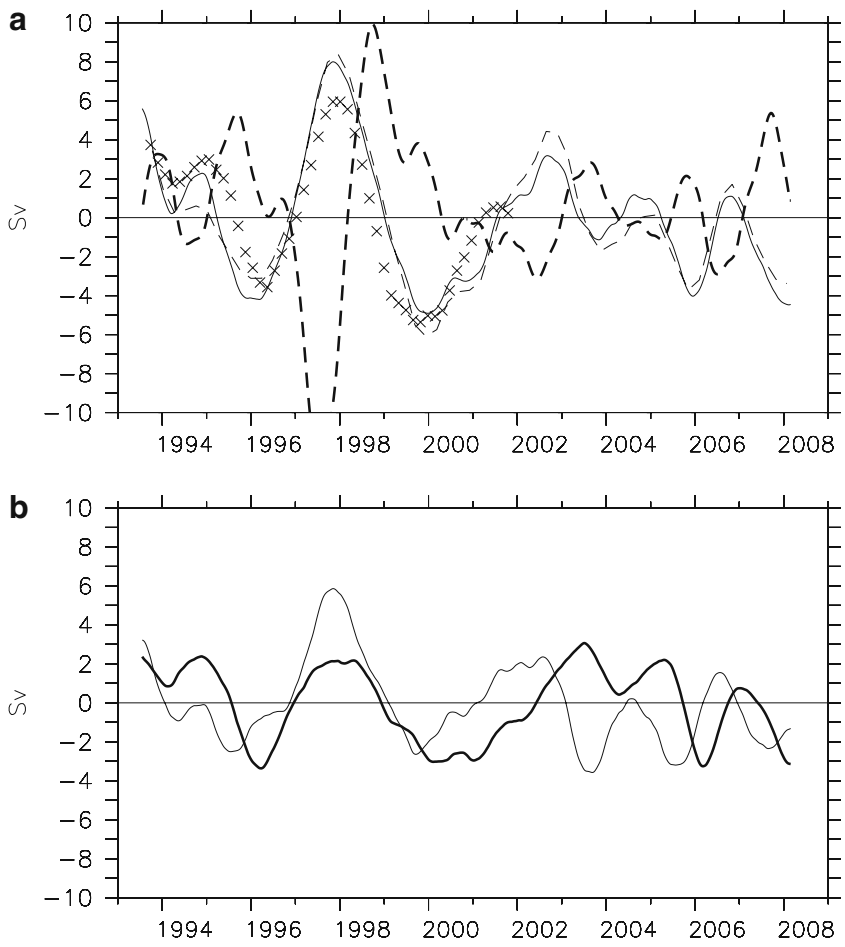

Fig. 11 **a** Time evolution of transport anomalies at the southern entrance of the Solomon Sea estimated by the SLA difference between PNG and Solomon Island and an e-folding depth of 150 m (*thin line*). The cumulative transport anomalies estimated in the same way for the Vitiaz and Solomon Straits are shown by a *thin dashed line*. Warm water volume changes in the western equatorial Pacific (dWWVw/dt) are shown by a *thick dashed line*. *Crosses* represent the estimate for the cumulated transport anomalies in western boundary currents as defined for Milne Bay (A2) and for the eastern tip of Woodlark (A1) using an e-folding of 200 m. **b** The time evolution for transport anomalies estimated for the Vitiaz Strait and for the Solomon Strait using the SLA difference on both sides of the straits and an e-folding depth of 150 m are shown with *thick* and *thin lines*, respectively. The units are shown in Sv

vertical structure of the mean LLWBCs with their core at the thermocline level, their variability is mainly explained by a first baroclinic mode. Altimetry may be used as a proxy to estimate anomalies of transport transiting in the Solomon Sea. At interannual time scale, the LLWBcs of the south Pacific counterbalance most of the changes of the warm water volume of the western equatorial Pacific, in phase with ENSO.

5 Variability in the eastern Solomon Sea: eddy activity

The large region of high variability surrounding the Solomon Sea, encompassing the South Equatorial Countercurrent (SECC) that extends eastward from the Solomon Islands at approximately 8°S (Gouriou and Toole 1993), has been studied by Qiu and Chen (2004). These authors indicated that the seasonal modulation of the EKE field was explained by a barotropic instability that is associated with horizontal shear in the SECC-SEC system. Such a current system cannot explain the large EKE signature observed in the Solomon Sea where the SECC is not present.

We focused our attention on the northeastern part of the Solomon Sea that exhibits the highest levels in SLA variability and EKE (Fig. 4). The patch of SLA variability is centered at 7°S–153°E, has a diameter of roughly 180 km, and displays intensity in terms of SLA that reach ~12 cm rms (~9 cm rms are associated with an interannual signal and ~5 cm rms with an annual signal). High EKE levels are associated with this patch of sea level variability. EKE averaged between 152°E–155°E; 8°S–5°S are characterized by a mean as high as 682 cm^2/s^2. This value integrates a high-frequency signal characteristic of meso-scale variability and a possible low frequency variability in the mean condition. To separate the contribution due to meso-scale activity from lower frequency variability, the SLA signal is high (half power at 180 days) and low (half power at 18 months) pass filtered, and both contributions to the EKE signal are presented in Fig. 12a. The meso-scale activity is the main contribution to the EKE signal with a mean of 340 cm^2/s^2. The low frequency component of the EKE signal is at a relatively low level (mean of 168 cm^2/s^2) except during the year 1998 where it reaches 1000 cm^2/s^2. It could be explained by drastic changes in the mean condition.

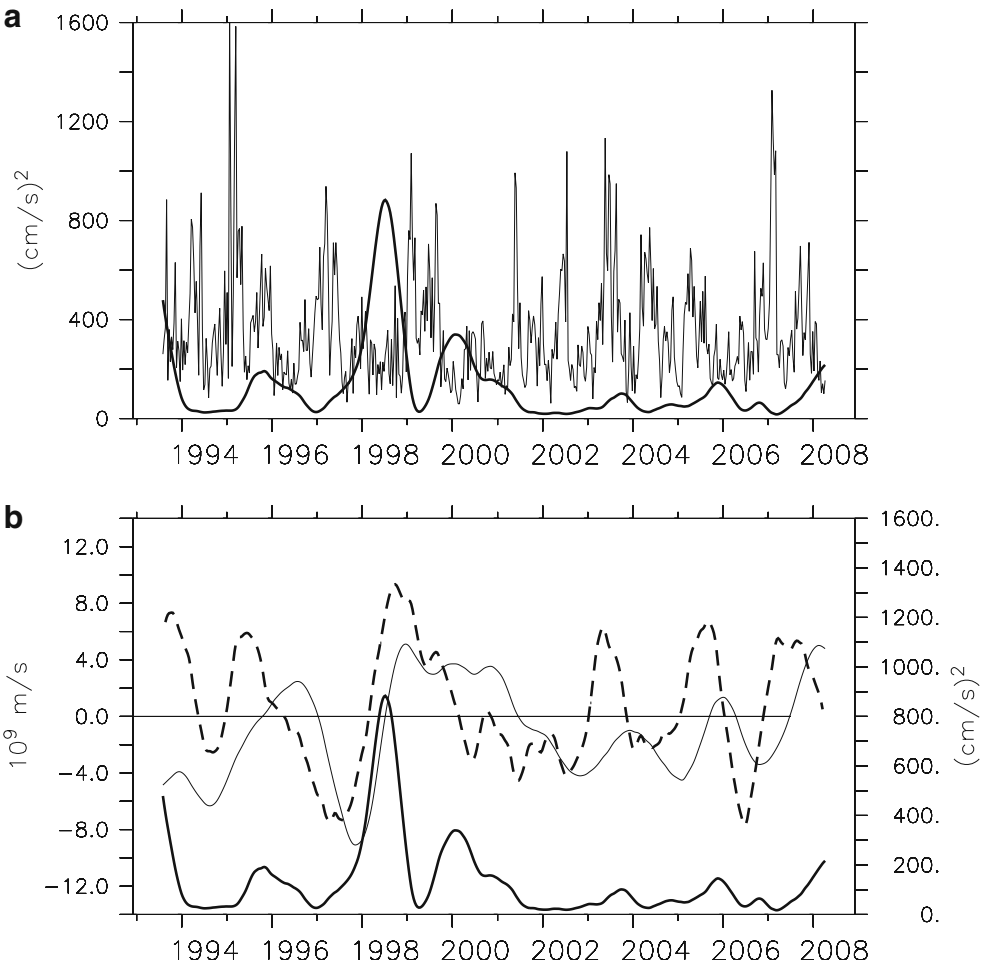

Fig. 12 **a** Time evolution of EKE averaged over 152°E–155°E; 8°S–5°S for the meso-scale component (*thin line*, the high-pass filter for SLA has a half power at 180 days) and the low frequency component (*thick line*, the low pass filter for SLA has a half power at 18 months). The units are cm^2/s^2. **b** Time evolution of the low frequency component of EKE (*black line*, the units are cm^2/s^2), of dSLA/dt over the Solomon Sea (*dash line*, the units are meters per second), and of the south oscillation index (*thin line*, for convenience, the 3*SOI is plotted)

The meso-scale activity appears to be modulated at lower frequency, especially at annual time scale. The spatial distribution of the meso-scale activity looks very much like the EKE distribution in Fig. 4b extending from the north to the south in the mid-basin (not shown). The maximum of kinetic energy corresponds to the maximum of annual variability in SLA at 7°S–153°E (Fig. 6). It is at its maximum during the austral autumn period when an anticyclonic current anomaly is developed that enhanced the mean southward flow from the SEC. In austral spring, the situation is opposite with a cyclonic eddy anomaly and a lower meso-scale activity. It suggests that the meso-scale activity in the Solomon Sea could be related to instabilities of the SEC branch entering the Solomon Sea at the Solomon strait.

The low frequency component of the EKE signal depends on ENSO activity, and during the 1993–2008 period, it was mainly dominated by one peak associated with the 1997–1998 ENSO event (Fig. 12b). In fact, it was low during the mature phase of ENSO, and it increased a few months after a peak in an El Niño event. The low frequency EKE signal was concentrated to the north in the double cells of high EKE shown in Fig. 3b and corresponded to a huge cyclonic anomaly at the mouth of the Solomon strait that was present during 6 months or more (1 year for the 1997–1998 ENSO event) after the mature phase of ENSO (Fig. 13). In fact, this cyclonic circulation corresponded with the phase transition between El Niño and La Niña, when the SLA in the Solomon Sea suddenly increased. It is noteworthy that the low frequency component of the EKE signal was not directly related to the SLA variability but to the speed at which the Solomon Sea was deplete or is replete (dSLA/dt). It suggests that it was dependent on the conditions outside the Solomon Sea. During the El Niño phase, eastward current anomalies depleted the western equatorial Pacific, whereas more to the southwestward current anomalies fed the LLWBCs of the Solomon Sea closing the circulation of current anomalies. It was a time period where the EKE activity was not related to its low frequency component. The transition phase between El Niño and La Niña can be defined here by a complex situation where westward current anomaly always entered the Solomon Sea by the south when westward current anomaly, characteristic of La Niña condition, prevailed in the equatorial band. In the Solomon Sea, the difficulty in flow exit through the straits contributes to enhance eddy

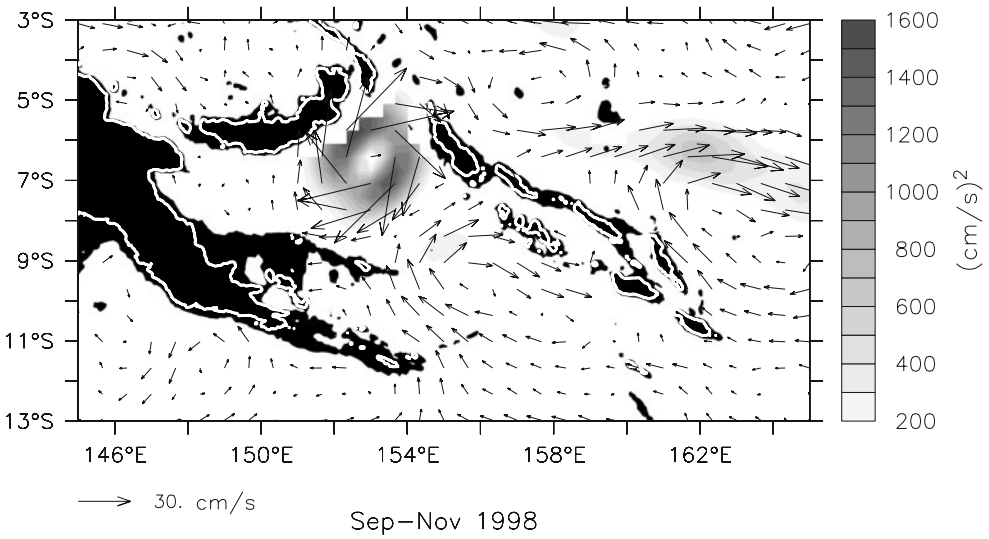

Fig. 13 Longitude/latitude plot of the low frequency component of EKE at the time of maximum EKE for the September to November 1998 period (*gray shading*). Units are cm^2/s^2. Superimposed are the corresponding surface anomalies of the geostrophic velocity field during the same time period. The land and the first 500 m oceanic depth are in *black*; the *white line* delineates the coastline

activity in the Solomon Sea in front of the Solomon Strait until the reverse of the current anomalies on the south.

The Solomon Sea with eddy mixing associated both to the strong meso-scale activity and to well developed eddies related to ENSO could play a significant role in water mass transformations between the subtropics and the equator.

6 Summary and conclusions

In this work, we present an analysis of the variability in the Solomon Sea using altimeter data. Our study was motivated by the fact that this specific region of the western tropical Pacific Ocean is a key region for oceanic climate connections between the equator and the subtropics. Additionally, the Solomon Sea is not often studied by conventional means and, at present, are only space observations able to provide a synoptic view for the area. Finally, the highest sea level variabilities observed for the south tropical Pacific were precisely concentrated in the Solomon Sea area and provide a strong incentive for looking at the altimeter signal in the region.

Since the Solomon Sea is quite a complex area from the bathymetric point of view, the adequacy of standard mapped (and relatively smooth) products for altimetry (i.e., AVISO data) may be in question. As a result, we also considered additional data from T/P tracks passing over the area, and a specific reprocessing from CTOH/LEGOS of along-track data was applied in order to potentially gain additional and more accurate information especially in the coastal area. The new dataset is helpful for defining and documenting coastal LLWBCs at annual and interannual time scales.

The overall surface variability in the Solomon Sea basin is under the influence of the surrounding large-scale ocean. Annual and interannual variability signals were strongly correlated with the outside ocean, in particular, at ENSO frequencies. At annual time scales, the Rossby wave signal at the latitude of the Solomon Strait controlled the signal inside the Solomon Sea. A specific feature characterizes the Solomon Sea which can be separated between a western basin (location of western boundary currents), characterized by relatively low sea level variability, and an eastern basin, characterized by an intense eddy activity. With the western and eastern Solomon Sea moving in phase, differences in SLA amplitudes between both sides yield SLA gradients that induce surface geostrophic current variations in the Solomon Sea in phase with the SLA signal.

At annual time scales, the SLA cycle induces a maximum southeastward surface geostrophic velocity anomaly during March to April in the Solomon Sea that produces a decrease in the NGCC. The opposite situation exists in September to October. The along-track analysis reveals the fine structure of the NGCC whose width is roughly 80 km. A 2-month phase lag exists between this current at the Vitiaz Strait and at Milne Bay. In accordance with anomaly in the NGCC, current anomalies were also detected along the southern coast of New Britain. Noteworthy is that the geostrophic current anomaly at the surface, as deduced from altimetry, revealed a circulation picture which was quite close to the annual thermocline circulation proposed by (Melet et al. 2010), as based on 1/12° resolution numerical simulations. It suggests that the western boundary currents, with their core in the subsurface at the thermocline level, have a variability with a strong signature at the surface characteristic of a first baroclinic mode.

At interannual time scales, the SLA variation in the Solomon Sea is typical of the basin-scale first ENSO mode. The SLA difference between both sides of the Solomon Sea

helped us to estimate variability in transport in the Solomon Sea (Ridgway et al. 1993). The model was used in ENSO event. Anomalies in the LLWBC counterbalance WWVw changes (dWWVw/dt). The growing phase of ENSO was characterized by a northward LLWBC flux in order to compensate for depletion of the WWVw. It confirmed the phasing of the LLWBC of the South Pacific to ENSO as suspected from previous modeling studies (Kug et al. 2003; Lee and Fukumori 2003; Ishida et al. 2008) with LLWBC anomalies in phase opposition with the interior geostrophic flow. The transport anomalies at the south Solomon Sea boundary were not similarly distributed between both the Vitiaz and Solomon straits. The highest transport anomalies were observed at the Solomon strait and were out of phase with the transport anomalies at the Vitiaz strait except during the 1997–1998 ENSO event.

High EKE is located at the north of the Solomon Sea and extends to the south at mid-basin. The meso-scale activity (intra seasonal frequencies) in the Solomon Sea is dominant, and it is modulated at annual period. Its location along the branch of the SEC, entering the Solomon Sea at the Solomon strait, argues for instabilities of this southward flow. The EKE signal has also a low frequency component that is dependent on ENSO activity with a main peak in 1998. This signal is particularly active during the phase transition between El Niño and La Niña when the oceanic condition outside the Solomon Sea prevents the anomalies in the Solomon Sea to easily escape. During this time period, a well-marked cyclonic signature is present at the mouth of the Solomon strait. Such structures associated with strong eddy mixing should contribute to significant water mass transformations. Future investigations are required to pinpoint such a mechanism of importance in a climate point of view when regarding the role of the LLWBC of the South Pacific to carry heat anomalies from the subtropics to the equator.

To conclude, altimetry appears as a valuable source of information for the variability in the low latitude boundary current system, but from an observational point of view, our study raises an issue regarding the limitations of standard altimeter products. Likely is that the study of such a region will strongly benefit from the advent of altimeter satellite missions by enforced capabilities near coasts (such as the SARAL/AltiKa mission to be launched in 2010, see Vincent et al. 2006) and even more from high-resolution-wide swath altimetry missions (such as those proposed by the SWOT project).

Acknowledgement This work was supported by the Centre National d'Etudes Spatiales (CNES). It is a contribution to the INSU/LEFE national programme and to the CLIVAR/SPICE International programme. Gridded altimeter products were produced by Ssalto/Duacs and distributed by AVISO, with support from Cnes (http://www.aviso.oceanobs.com/duacs). The original T/P data were reprocessed at the Center for Topographic studies of the Oceans and Hydrosphere (CTOH/LEGOS, http://www.legos.obs-mip.fr/fr/observations/ctoh). We thank Florence Birol for her help reprocessing the altimeter data, Billy Kessler, Sophie Cravatte, and Patrick Marchesiello for their helpful comments. WWV time series were obtained from the TAO Project Office at NOAA/PMEL (http://www.pmel.noaa.gov/tao/elnino/wwv/).

References

Alory G, Delcroix T (2002) Interannual sea level changes and associated mass transports in the tropical Pacific from TOPEX-Poseidon data and linear model results (1964-1999). J Geophys Res 107(C10):1999. doi:10.1029/2001JC001067

Barnier B et al (2006) Impact of partial steps and momentum advection schemes in a global ocean circulation model at eddy-permitting resolution. Ocean Dyn 56(5–6):543–567. doi:10.1007/s10236-006-0082-1

Butt J, Lindstrom E (1994) Currents off the east coast of New Ireland, Papua New Guinea, and their relevance to regional undercurrents in the western equatorial Pacific ocean. J Geophys Res 99(C6):12 503–12 514

Carrere L, Lyard F (2003) Modeling the barotropic response of the global ocean to atmospheric wind and pressure forcing—comparisons with observations. Geophys Res Lett 30(6):1275. doi:10.1029/2002GL016473

Chen S, Qiu B (2004) Seasonal variability of the South Equatorial Countercurrent. J Geophys Res 109:C08003. doi:10.1029/2003JC002243

Durand F, Shankar D, Birol F, Satheesh Chendra Shenoi S (2008) Estimating boundary currents from satellite altimetry: a case study for the east coast of India. J Oceanogr 64:831–845

Gourdeau L, Kessler WS, Davis RE, Sherman J, Maes C, Kestenare E (2008) Zonal jets entering the coral sea. J Phys Oceanogr 38:715–725

Gouriou Y, Toole J (1993) Mean circulation of the upper layers of the western equatorial Pacific ocean. J Geophys Res 98 (22):495

Ishida A, Hosoda S, Ando K (2008) North-south asymmetry of warm water volume transport related with El Nino variability. Geophys Res Letter 35:L18612. doi:10.1029/2008GL034858

Jin F (1997) An equatorial ocean recharge paradigm for ENSO, part I: conceptual model. J Atmos Sci 54:811–829

Kessler WS, Gourdeau L (2007) The annual cycle of circulation of the Southwest subtropical Pacific, analysed in an ocean GCM. J Phys Oceanogr 37:1610–1627

Kug JS, Kang IS, An SI (2003) Symmetric and antisymmetric mass exchanges between the equatorial and off-equatorial Pacific associated with ENSO. J Geophys Res 108(C8):3284

Kuroda Y (2000) Variability of currents off the northern coast of New Guinea. J Oceanogr 56:103–116

Lee T, Fukumori I (2003) Interannual to decadal variation of tropical-subtropical exchange in the Pacific Ocean: boundary versus interior pycnocline transports. J Climate 16:4022–4042

Lindstrom E, Lukas R, Fine R, Firing E, Godgrey S, Meyers G, Tsuchiya M (1987) The western equatorial ocean circulation study. Nature 330:533–537

Lindstrom E, Butt J, Lukas R, Godfrey S (1990) The flow through Vitiaz strait and St Georges's channel, Papua New Guinea. In: Pratt LJ (ed) The physical oceanography of sea strait. Kluwer Academic Publishers, Dordrecht, pp 171–189

Lübbecke JF, Böning CW, Biastoch A (2008) Variability in the subtropical-tropical cells and its effect on near-surface

temperature of the equatorial Pacific: a model study. Ocean Sci 4:73–88

Luo Y, Rothstein L, Zhang R, Busalacchi A (2005) On the connection between South Pacific subtropical spiciness anomalies and decadal equatorial variability in an ocean general circulation model. J Geophys Res 110(10):002

Lyard F, Lefevre F, Letellier T, Francis O (2006) Modelling the global ocean tides: modern insights from FES2004. Ocean Dyn 56:349–415

Maes et al. (2009) Rapport de la mission océanographique FLUSEC-01 à bord du N. O. Alis du 12 au 30 Août 2007 en mer de Corail, Océan Pacifique Sud-Ouest: IRD, (Sciences de la Mer. Oceanographie Physique. Rapports de Convention, N°24), 98 pp

Meinen CS (2005) Meridional extent and interannual variability of the Pacific Ocean tropical-subtropical warm water exchange. J Phys Oceanogr 35(3):323–335

Meinen CS, McPhaden MJ (2001) Interannual variability in warm water volume transports in the equatorial Pacific during 1993-1999. J Phys Oceanogr 31:1324–1345

Melet A, Gourdeau L, Kessler W, Verron J, Molines J (2010) Thermocline circulation in the Solomon Sea: a modeling study. J Phys Oceanogr 18pp (in press). doi:10.1175/2009JPO4264.1

Murray S, Lindstrom E, Kindle J, Weeks E (1995) Transport through Vitiaz Strait. WOCE notes, 7

Pascual A, Faugère F, Larnicol G, Le Traon PY (2006) Improved description of the ocean mesoscale variability by combining four satellite altimeters. Geophys Res Let 33: L02611

Qiu B, Chen S (2004) Seasonal modulations in the Eddy field of the South Pacific Ocean. J Phys Oceanogr 34:1515–1527

Qu T, Lindstrom E (2002) A climatological interpretation of the circulation in the Western South Pacific. J Phys Oceanogr 32:2492–2508

Ridgway KR, Godfrey JS, Meyers G, Bailey R (1993) Sea level response to the 1986-1987 El Nino Southern Oscillation event in the Western Pacific in the vicinity of Papua New Guinea. J Geophys Res 98:16 387–16 395

Roblou L, Lyard F, LeHenaff M, Maraldi C (2007) X-TRACK, a new processing tool for altimetry in coastal oceans. Envisat Symposium 2007, Montreux, Switzerland, ESA SP-636, July 2007

Schneider N (2004) The response of the tropical climate to the equatorial emergence of spiciness anomalies. J Climate 17:1083–1095

Tomczak M, Godfrey J (1993) Regional oceanography: an introduction. Pergamon Press, Great Britain

Tsuchiya M, Lukas R, Fine R, Firing E, Lindstrom E (1989) Source waters of the Pacific Equatorial Undercurrent. Prog Oceanogr 23:101–147

Ueki I, Kashino Y, Kuroda Y (2003) Observation of current variations off the New Guinea coast including the 1997–1998 El Nino period and their relationship with Sverdrup transport. J Geophys Res 108(C7):36-1–36-17. doi:10.1029/2002JC001611

Vincent P, Steunou N, Caubet E, Phalippou L, Rey L, Thouvenot E, Verron J (2006) AltiKa: a Ka-band altimetry payload and system for operational altimetry during the GMES period. Sensors 6:208–234

Wunsch C, Stammer D (1995) The global frequency-wavenumber spectrum of oceanic variability estimated from TOPEX/POSEIDON altimetric measurements. J Geophys Res 100 (C12):24,895–24,910

Yeager SG, Large WG (2004) Late-winter generation of spiciness on subducted isopycnals. J Phys Oceanogr 34:1528–1545